IUPAC Task Group on Atmospheric Chemical Kinetic Data Evaluation – Data Sheet P1

The citation for this datasheet is: Atkinson, R., Baulch, D. L., Cox, R. A., Crowley, J. N., Hampson, R. F., Hynes, R. G., Jenkin, M. E., Rossi, M. J., and Troe, J.: Atmos. Chem. Phys. 4, 1461, 2004; IUPAC Subcommittee for Gas Kinetic Data Evaluation, (http://iupac.pole-ether.fr).
This datasheet updated: 16th April 2013; last change in preferred values: 16th April 2013

HCHO + hυ → products

Primary photochemical transitions

Reaction		$\Delta H°_{298}$/kJ·mol^{-1}	$\lambda_{threshold}$/nm
HCHO + hυ → H + HCO	(1)	369.7	324
→ H_2 + CO	(2)	-1.9	

Absorption cross-section data

Wavelength range/nm	Reference	Comments
240 – 360	Moortgat and Schneider, 1988	(a)
300 – 360	Cantrell et al., 1990	(b)
225 – 375	Meller and Moortgat, 2000	(c)
308 – 320	Pope et al., 2005a, 2005b	(d)
300 - 340	Smith et al., 2006	(e)
240 – 370	Gratien et al., 2007	(f)
304 – 330	Tatum Ernest et al.,, 2012	(g)

Quantum yield data ($\phi = \phi_1 + \phi_2$)

Measurement	Wavelength /nm	Reference	Comments
ϕ, ϕ_2/ϕ	253-353	Moortgat et al., 1983	(h)
ϕ_1	269-339	Smith et al., 2002	(i)
$\phi_1 = 0.71 \pm 0.08$	308.86	Pope et al., 2005a, 2005b	(j)
$= 0.69 \pm 0.07$	314.13		
$\phi_1 = 0.62 \pm 0.09$	303.70	Gorrotxategi et al., 2008	(k)
0.57 ± 0.10	306.13		
0.61 ± 0.08	308.78		
0.69 ± 0.06	314.31		
0.64 ± 0.10	320.67		
0.51 ± 0.10	325.59		
0.28 ± 0.11	329.51		
$\phi_1 = 0.697 \pm 0.081$	306.6	Tatum Ernest et al., 2012	(l)
0.746 ± 0.087	309.7		
0.594 ± 0.069	312.4		
0.690	315.0		
0.534 ± 0.062	318.1		
0.326 ± 0.038	321.3		
0.630 ± 0.073	323.9		
0.504 ± 0.059	326.7		

Comments

(a) Cross-sections measured at 220 K and 298 K at different concentrations of HCHO and extrapolated to zero concentration. This extrapolation procedure yielded virtually identical cross-sections with and without added N_2.

(b) High-resolution FT spectroscopy used to measure cross-sections as a function of temperature (223 to 293 K). Values at different *p*(HCHO) were extrapolated to zero concentration. Cross-section measurements with resolution of 0.025 nm at selected temperatures between 223-323 K. HCHO pressure kept below 0.65 mbar to avoid saturation effects. Error limits on $\sigma \pm 5\%$ and on temperature coefficients < 8%.

(c) High resolution (~0.025 nm) absorption spectrum of HCHO measured using diode array spectroscopy over wide wavelength range. Temperature: 298 and 223 K.

(d) High resolution spectrum measured by tunable UV laser absorption spectroscopy in the range 308 - 320 nm, at 263K and 294K. The spectrometer was designed to study the photolysis of HCHO, using CRDS to detect HCO photoproduct, while simultaneously measuring HCHO absorption cross sections, at resolution close to the limit of Doppler broading of 0.07 cm^{-1}. The spectral features were sharper and the measured peak cross sections were larger than reported for the previous studies (b) and (c); however the integrated intensities in a particular band were in good agreement. Quenching effect of increasing *p*(HCHO) above 1.3 mbar on cross sections was observed.

(e) As (d) but wavelength range extended to 300 - 340 nm at 294 and 245 K. Addition of N_2 or O_2 up to 660 mbar had only small effects on cross sections and widths of the spectral features measured at the high resolution used.

(f) UV/IR spectra of HCHO in 1 bar N_2 were simultaneously recorded in a multipass White cell equipped with a conventional UV spectrometer (resolution of 0.15 nm) and FTIR system (0.1

cm^{-1}). UV cross-sections were deduced from infrared absorption coefficients measured separately by FTIR in a stainless steel photoreactor.

(g) Absorption cross sections for the $\tilde{A}^1A_2 - \tilde{X}^1A_1$ electronic transition of formaldehyde measured at 294 ± 2 K over the spectral range 30285−32890 cm^{-1} (304−330 nm) using UV laser absorption spectroscopy; resolution better than 0.09 cm^{-1}. Pressure broadening parameters were obtained for the collision partners He, O_2, N_2, and H_2O; pressure broadening coefficient for H_2O was an order of magnitude larger than the coefficients for O_2 and N_2.

(h) Quantum yields of CO and H_2 were measured as a function of wavelength for HCHO in low concentration in air. Previous results showing the pressure and temperature dependences of ϕ_1 and ϕ_2 were confirmed.

(i) The relative quantum yield for the production of radical products, H and HCO, measured directly using an NO-chemical amplification method, with subsequent detection of NO_2^- by CIMS. All yields were measured at a pressure of 50 Torr (66 mbar) and were normalized to a quantum yield of $\phi_2 = 0.753$ at 303.75 nm based on the recommendation of DeMore *et al*. (1997). The quantum yields were measured with sufficient wavelength resolution (± 0.62 nm, fwhm) to observe structure that had not been previously reported.

(j) Using same experimental system as described in (d) at seven wavelengths in range 303.75 - 329.51. Relative quantum yields measured at high resolution observed to be wavelength dependent within single bands in the 313 - 320 nm region; absolue quantum yields cited were obtained by normalising to literature value in the same manner as Smith et al (2002).

(k) Using same experimental system as (d) to determine the yields of HCO produced by photolysis using CRDS. Absolute quantum yields for the radical channel, $\phi_1(\lambda)$, measured at seven wavelengths using an independent calibration technique based on simultaneous photolysis of HCHO and Cl_2, and a model of the post-photolysis chemistry. The absolute uncertainties of the measured values of ϕ_1 was between 0.06 and 0.11, estimated by combining the precision on ϕ_1 with the uncertainty in the $\sigma_{HCHO}(\lambda)$ values (5 to 10%). These absolute values of $\phi_1(\lambda)$ were used with the measured values of $\sigma_{HCHO}(\lambda)$ to scale an extensive set of relative HCO yield measurements. This procedure provided a full suite of data for the product: $\sigma_{HCHO}(\lambda) \times \phi_{HCO}(\lambda)$ at wavelengths from 302.6 to 331.0 nm, at wavelength resolution of 0.005 nm (an 'action spectrum'). However this procedure resulted in increased uncertainty in the quantum yields derived in regions of low $\sigma(\lambda)$.

(l) The relative quantum yield for the production of radical products, H + HCO, from the UV photolysis of formaldehyde (HCHO) was measured using a PLP−PLIF technique over the wavelength region 304−329 nm. The photolysis laser had a bandwidth of 0.09 cm^{-1}. The H and HCO photo-fragments were monitored by conversion to HO by their rapid reaction with NO_2. The HO spectroscopic marker was detected at high sensitivity by LIF. This technique produced an "action" spectrum of the product $\sigma_{HCHO}(\lambda) \times \phi_{HCO}(\lambda)$ as a function of photolysis wavelength. The relative quantum yields were determined from the action spectrum using the HCHO absorption cross sections averaged over each 100 cm^{-1}, previously obtained in their laboratory. Yields were normalized to a value of 0.69 at 31,750 cm^{-1} based on the current NASA recommendation (Sander *et al.* (2011)). The resulting radical quantum yields agree well with previous experimental studies but show greater wavelength dependent structure than reported from the previous experimental studies of Smith *et al.* (2002) and Gorrotxategi *et al.* (2008) at high resolution.

Preferred Values

Absorption cross-sections at 298 and 223 K Averaged Over Intervals Used in Atmospheric Modelling

Wavelength* / nm	Wavelength Range,* / nm	10^{20} σ(298 K) cm^2	10^{20} σ(223 K) cm^2	10^{24} Γ cm^2 K^{-1}
226.0	224.7-227.3	0.017		
228.6	227.3-229.9	0.018		
231.3	229.9-232.6	0.030		
234.0	232.6-235.3	0.032		
236.7	235.3-238.1	0.063		
239.6	238.1-241.0	0.071		
242.5	241.0-243.9	0.127		
245.4	243.9-246.9	0.139		
248.5	246.9-250.0	0.254		
251.7	250.0-253.3	0.270	0.264	0.76
254.9	253.3-256.4	0.456	0.443	1.78
258.1	256.4-259.7	0.477	0.436	5.40
261.5	259.7-263.2	0.703	0.693	1.35
265.0	263.2-266.7	0.738	0.701	4.97
268.5	266.7-270.3	1.129	1.107	2.86
272.2	270.3-274.0	1.292	1.263	3.88
275.9	274.0-277.8	1.844	1.887	-5.64
279.8	277.8-281.7	1.859	1.887	-3.76
283.7	281.7-285.7	2.556	2.724	-22.43
287.8	285.7-289.9	2.310	2.361	-6.90
292.0	289.9-294.1	2.665	2.932	-35.58
296.3	294.1-298.5	3.294	3.252	5.54
300.8	298.5-303.0	1.605	1.585	2.55
305.4	303.0-307.7	4.394	4.406	-1.56
310.1	307.7-312.5	1.632	1.674	-5.58
315.0	312.5-317.5	4.085	4.023	8.30
320.0	317.5-322.5	1.529	1.468	8.15
325.0	322.5-327.5	2.791	2.761	3.94
330.0	327.5-332.5	1.989	1.909	10.59
335.0	332.5-337.5	0.196	0.183	1.71
340.0	337.5-342.5	2.387	2.273	15.24
345.0	342.5-347.5	0.759	0.755	0.51
350.0	347.5-352.5	0.195	0.220	-3.43
355.0	352.5-357.5	0.960		
360.0	357.5-362.5	0.014		
365.0	362.5-367.5	0.010		
370.0	367.5-372.5	0.037		

* Wavelengths are calibrated in air.

To calculate the UV absorption spectrum at a given temperature T, the following equation is used:

$$\sigma(\lambda, T) = \sigma(\lambda, 298\ \mathrm{K}) + \Gamma(T - 298\ \mathrm{K})$$

Absorption Cross Sections at 298 K, σ(298 K), Averaged Over 1 nm Intervals Centered at the Cited Wavelength, λ.

λ / nm *	10^{21} σ(298 K) cm^2	λ / nm *	10^{21} σ(298 K) cm^2	λ / nm *	10^{21} σ(298 K) cm^2
226	0.18	276	25.84	326	68.76
227	0.17	277	15.73	327	43.70
228	0.18	278	10.35	328	12.20
229	0.19	279	24.51	329	31.20
230	0.21	280	23.38	330	38.65
231	0.17	281	15.62	331	14.12
232	0.34	282	9.73	332	3.47
233	0.26	283	7.22	333	2.14
234	0.33	284	42.65	334	1.59
235	0.36	285	40.50	335	0.97
236	0.54	286	20.95	336	1.26
237	0.77	287	11.53	337	3.83
238	0.57	288	31.69	338	19.19
239	0.68	289	32.25	339	53.81
240	0.78	290	11.73	340	31.51
241	0.78	291	18.36	341	9.78
242	1.23	292	7.97	342	5.09
243	1.59	293	31.28	343	19.22
244	1.10	294	71.54	344	12.68
245	1.31	295	40.54	345	4.37
246	1.63	296	24.74	346	1.19
247	1.51	297	13.67	347	0.44
248	2.34	298	42.17	348	0.75
249	3.18	299	31.75	349	0.38
250	2.57	300	9.64	350	0.36
251	2.04	301	16.25	351	0.89
252	3.37	302	8.54	352	7.30
253	2.89	303	30.21	353	22.75
254	3.42	304	72.19	354	16.45
255	4.50	305	47.52	355	6.96
256	6.28	306	42.92	356	1.48
257	4.43	307	17.81	357	0.35
258	3.07	308	13.85	358	0.19
259	6.17	309	32.52	359	0.11
260	6.05	310	17.37	360	0.09
261	6.59	311	4.62	361	0.10
262	6.03	312	11.88	362	0.21
263	10.77	313	9.06	363	0.14
264	9.47	314	56.37	364	0.09
265	5.31	315	55.65	365	0.09
266	5.39	316	25.61	366	0.09
267	13.60	317	57.77	367	0.09
268	12.43	318	31.51	368	0.14
269	9.91	319	9.78	369	0.30
270	9.63	320	11.94	370	0.64
271	19.41	321	15.98	371	0.57
272	14.30	322	7.22	372	0.20
273	8.11	323	3.28	373	0.11
274	6.58	324	8.58	374	0.09
275	21.43	325	15.78	375	0.09

*Wavelengths are calibrated in air.

Quantum yields in air at 1 bar and 298 K

λ/nm	ϕ_1	ϕ_2	ϕ_{total}	λ/nm	ϕ_1	ϕ_2	ϕ_{total}
240	0.270	0.730	0.800	318	0.660	0.340	1.000
250	0.320	0.480	0.800	319	0.579	0.431	1.000
260	0.310	0.490	0.800	320	0.600	0.400	1.000
269	0.400	0.410	0.810	321	0.650	0.350	1.000
279	0.560	0.320	0.880	322	0.580	0.420	1.000
280	0.580	0.300	0.880	323	0.475	0.525	1.000
281	0.600	0.270	0.870	324	0.490	0.510	1.000
282	0.620	0.270	0.890	325	0.460	0.540	1.000
283	0.640	0.250	0.890	326	0.506	0.494	1.000
284	0.650	0.260	0.910	327	0.500	0.500	1.000
285	0.670	0.310	0.980	328	0.400	0.600	1.000
286	0.680	0.320	1.000	329	0.329	0.671	1.000
287	0.700	0.300	1.000	330	0.380	0.620	1.000
288	0.710	0.290	1.000	331	0.460	0.430	0.890
289	0.710	0.290	1.000	332	0.370	0.450	0.820
290	0.720	0.280	1.000	333	0.240	0.480	0.720
291	0.730	0.270	1.000	334	0.112	0.510	0.622
292	0.730	0.270	1.000	335	0.070	0.560	0.630
293	0.740	0.260	1.000	336	0.055	0.620	0.675
294	0.700	0.300	1.000	337	0.035	0.610	0.645
295	0.790	0.210	1.000	338	0.010	0.580	0.590
296	0.760	0.240	1.000	339	0.011	0.580	0.591
297	0.740	0.280	1.000	340	0.010	0.640	0.650
298	0.670	0.330	1.000	341	0.008	0.610	0.618
299	0.650	0.350	1.000	342	0.008	0.580	0.588
300	0.700	0.300	1.000	343	0.008	0.550	0.558
301	0.700	0.300	1.000	344	0.007	0.510	0.517
302	0.730	0.270	1.000	345	0.007	0.500	0.507
303	0.714	0.286	1.000	346	0.007	0.470	0.477
304	0.750	0.250	1.000	347	0.007	0.440	0.447
305	0.710	0.290	1.000	348	0.007	0.420	0.427
306	0.642	0.358	1.000	349	0.006	0.380	0.386
307	0.680	0.320	1.000	350	0.006	0.360	0.366
308	0.700	0.300	1.000	351	0.005	0.330	0.335
309	0.710	0.290	1.000	352	0.005	0.300	0.305
310	0.700	0.300	1.000	353	0.005	0.280	0.285
311	0.680	0.320	1.000	354	0.005	0.250	0.255
312	0.669	0.331	1.000	355	0.005	0.120	0.125
313	0.730	0.270	1.000	356	0.000	0.100	0.100
314	0.681	0.319	1.000	357	0.000	0.070	0.070
315	0.780	0.220	1.000	358	0.000	0.040	0.040
316	0.750	0.250	1.000	359	0.000	0.010	0.010
317	0.653	0.347	1.000	360	0.000	0.000	0.000

Pressure dependence of quantum yields in air

240 – 330 nm: ϕ_1 and ϕ_2 values independent of temperature and pressure.
330 – 360 nm: ϕ_1 values independent of temperature and pressure. ϕ_2 values are subject to Stern-Volmer pressure quenching:

$$1/\phi_2 = 1 + (k_q/k_d)\ x[M]$$

where [M] is the concentration of air molecules. The quenching coefficients (k_q/k_d /cm^{-3} molecule^{-1}) increase with decreasing temperature and wavelength. Recommended values for HCHO mixtures in air at 300K and 220K given below:

Recommended quenching coefficients for ϕ_2

Wavelength/nm	Temperature/K	
	300 $10^{19}\,k_q/k_d$ /cm^{-3} molecule^{-1}	220 $10^{19}\,k_q/k_d$ /cm^{-3} molecule^{-1}
329	0.26 ± 0.10	1.12 ± 0.17
353	0.39 ± 0.07	2.47 ± 0.59

Comments on Preferred Values

The photochemistry of HCHO in the near UV region has been intensively studied over a long period in view of the importance of HCHO photolysis for atmospheric chemistry. The UV spectrum consists of a series of discrete vibrational bands resulting from the $\tilde{A}\,^1A_2$–$\tilde{X}\,^1A_1$ electronic transition of HCHO in the wavelength range 240–360 nm.

Photolysis of HCHO in this wavelength region leads to two distinct product types: at wavelengths longer than the threshold for dissociation to H + HCO radicals, only 'molecular' products, H_2 + CO are formed; at shorter wavelengths both sets of products are formed, the relative yields depending on wavelength. Photodissociation involves both S^0 and T^1 excited states populated from the S^1 state produced initially by photo-excitation in the near UV. The yield of radical products, H + HCO, predominates in the region 280-320 nm.

Several studies have focussed on the structured region 290 – 330 nm at high resolution. Pope *et al.* (2005a and 2005b) reported results using LAS with resolution of 0.1 cm^{-1} (close to the Doppler broadening limit at 294 K of 0.07 cm^{-1}), which is sufficient to resolve the sharpest spectral features in the ro-vibrational spectrum of HCHO. Peak cross sections in the Pope et al. (2005) studies were up to 30% higher that obtained from the lower resolution studies. Smith *et al.* (2006) reported measurements from the same laboratory at resolution of 0.35 cm^{-1}, which show that cross sections at this resolution are unaffected by pressure of N_2. Absorption cross section measurements at high resolution have also been reported recently by Tatum Ernest et al. (2012a) at a resolution better than 0.09 cm^{-1}. This improves on the previously published data of Smith et al. (2006) (0.35 cm^{-1}) over the same region and agrees well with the regions obtained at sub-Doppler resolution by Motsch et al. (2008) and Crow et al. (2009). These studies show that the measured absorption cross sections are dependent on the bandwidth of the probe laser unless the bandwidth is significantly narrower than the Doppler line width. In general there is good consistency between the different results for the peak cross sections measured at high resolution, when these effects are taken into account.

Gratien et al. (2007a and b) measured UV absorption cross sections at 0.15 nm resolution and reported integrated band intensities (IBI) for the main vibronic bands in the range 240 - 370 nm. The IBI values compared well (within 7%) with earlier studies of

Cantrell et al. (1990), Meller and Moortgat, (2000), and with the more recent studies of Pope et al. (2005) and Smith et al. (2006) in the range 300-330 nm. Integrated Intensities for two regions around 30712 cm^{-1} and 30635 cm^{-1} in the $2_0^2 4_0^1$ vibronic band, measured in the study of Tatum Ernest *et al.* (2012a), agreed well with results from Crow et al. (2009) Cantrell et al. (1990), Meller and Moortgat, (2000), and Smith et al. (2006).

The cross section data up to 2011 have been evaluated by Calvert et al. (2008, 2011). They conclude that the data of Meller and Moortgat (2000), averaged over 1 nm intervals centered at the given wavelengths, are the most accurate of the available cross-section data for atmospheric photolysis rate calculations. The integrated band intensities from the results of Tatum Ernest *et al.* (2012a) support the validity of the cross sections of Meller and Moortgat (2000), which are the basis of the preferred values. The temperature dependence over the range 250-356 nm reported by Meller and Moortgat (2000) exhibits the same general changes on band shape as the previously recommended spectra but differs in the shape of the individual rotational bands. Resolution should not exceed 1 nm to assure correct representation of the temperature dependent cross sections.

The quantum yields ϕ_1 and ϕ_2 at atmospheric pressure and 298 K have been determined by Moortgat *et al*. (1983). Their results were consistent with earlier measurements of the quantum yields by Horowitz and Calvert (1978) Clark et al. (1978), Tang et al. (1979). The high resolution study of Smith et al. (2002) showed structure in the wavelength dependence of ϕ_1, indicated earlier in the work of Tang et al. (1979) in the region 303.7 - 328.9 nm. Other subsequent measurements of quantum yields for the 'radical' channel ϕ_1 at very high resolution confirm the presence of resolved fine structure in the yield of HCO radicals The relative quantum yields of Smith et al. (2002) were referenced to a value of $\phi_1 = 0.753$ at 303.75 nm recommended by DeMore et al. in JPL 97-4, (1997). Values of ϕ_1 reported by Pope et al. (2005b) and Tatum Ernest *et al.* (2012b), were referenced to a value of $\phi_1 = 0.690$ at 314.9 nm. The results of Gorrotxategi Carbajo et al. (2008) gave absolute HCO quantum yield values which were obtained using an independent calibration method based on the *in situ* UV photolysis of Cl_2 in the presence of HCHO. Their measurement at 314.7 nm is identical to the JPL recommendation at this wavelength (Sander et al. (2011)).

Overall, there is good general agreement between the high resolution studies, but there are some significant differences in detail. For example the ϕ_1 results of Gorrotxategi Carbajo et al. (2008) are lower by ~25% than those of Smith *et al.* (2002) and Tatum Ernest et al. (2012b) in the 303 - 309 nm wavelength interval. Also the results of Tatum Ernest et al. in the band centred at 321.3 nm are substantially lower than the other high resolution results. These differences may reflect the difficulty of averaging the high resolution data and the uncertainty in deriving single wavelength values of ϕ_1 by dividing the $\sigma \times \phi$ action spectra by individually measured σ values. The study of Tatum Ernest et al. (2012b) produced the higher quality spectra but nevertheless there was significant variability between the directly determined ϕ_1 values compared with band-averaged values. This study indicated greater wavelength dependent structure compared to the results of Smith et al. (2002), Pope et al. (2005) and Gorrotxategi Carbajo et al. (2008) (see Fig. 1).

Calvert et al. (2008, 2011) have evaluated the data for the quantum yields to produce recommended values of ϕ_1 at 1 nm intervals over the range 250-356 nm, estimated from the combined data sets of Moortgat et al. (1983), Horowitz and Calvert, (1978), Clark et al. (1978), and Smith et al. (2002). Values of ϕ_1 for each nm unit of λ were obtained by linear

extrapolation between sequential data points. A simple average was taken for measurements at the same wavelength, which were weighted equally. Data points recommended for $\lambda > 340$ nm and $\lambda < 268.75$ nm accepted the results of Moortgat et al. (1983) alone. The recommended values of ϕ_1 are independent of pressure. Their recommendations differ from those in the previous IUPAC (2004) in the 284-339 nm range, and from the latest JPL recommendation (Sander et al., 2011), which uses a polynomial fit to the data of Lewis et al. (1976), Marling (1977), Moortgat et al. (1983), Horowitz and Calvert, (1978), Clark et al. (1978), Tang et al. (1979), Smith et al. (2002), Pope et al. (2005a & b), and Gorrotxategi Carbajo et al. (2008). The JPL formulae give a smooth dependence of ϕ_1 on λ over the whole wavelength range.

Calvert et al. (2008, 2011) have evaluated these data and concluded that the total quantum yield $\phi_1 + \phi_2 = 1.0$ over the range 285 - 385 nm. For the current IUPAC recommendation we have adopted the values of ϕ_1 at 1 nm intervals from Calvert *et al.* (2011). To emphasize the structure dependence of ϕ_1 on λ , we have chosen to average, with equal weighting, the interpolated values from the newer high resolution results of Gorrotxategi Carbajo et al. (2008) and Tatum Ernest et al. (2012) into the 1 nm interval data, for the principle bands of HCHO absorption in the range 303.7 - 328.9 nm. This has the effect of increasing the amount of structure in the wavelength dependence of ϕ_1 (see fig 2).

The recommended values for ϕ_2 are obtained by the difference (ϕ_T - ϕ_1), where ϕ_T is the sum of the two channels (1) and (2) at 1 bar and 298 K, based on the data of Moortgat *et al*. (1983). Over the range 285 - 330 nm $\phi_T = \phi_1 + \phi_2 = 1.0$ and is independent of pressure and temperature. At $\lambda > 330$ nm the values of ϕ_2 are sensitive to pressure and temperature. The quenching follows the Stern-Volmer relation, $1/\phi_2 = 1 + (k_q/k_d)$ x[M], where [M] is the concentration of air molecules. The recommended quenching coefficients ((k_q/k_d), cm^{-3} $molecule^{-1}$) are the values given by Calvert et al. (2011) for HCHO mixtures in air for 300 K at 329 nm and 353 nm respectively: $(0.26 \pm 0.10) \times 10^{-19}$ and $(1.12 \pm 0.17) \times 10^{-19}$; constants for 220 K at 329 nm and 353 nm respectively are: $(0.39 \pm 0.07) \times 10^{-19}$ and $(2.47 \pm 0.59) \times 10^{-19}$. At $\lambda < 285$ nm the values of ϕ_T ($= \phi_1 + \phi_2$) were those of Moortgat et al. (1983), assumed independent of pressure. Figure 3 shows a plot of the wavelength dependence of preferred values of ϕ_1, ϕ_2 and ϕ_{total} over the range 240 - 360 nm.

The structure observed in the wavelength dependence of the quantum yields provides evidence for the complex competition among the various dissociation pathways of singlet and triplet excited state formaldehyde to give: H + HCO, H + H + CO and H_2 + CO, which has been diagnosed from numerous studies of the photo-dissociation dynamics of excited HCHO molecules. These studies reveal that several parallel unimolecular decomposition pathways exist, yielding the two sets of chemically distinct products: H + HCO (1) and H_2 + CO (2). Reaction (1) can occur *via* both S^0 and T^1 states, while reaction (2) occurs solely *via* S^0. Not only do the molecular and radical product channels compete, but distinct S^0 and T^1 pathways can lead to the same products, i.e H + HCO.

Troe (2007a) has analyzed the temperature and pressure dependencies of the experimental quantum yields at $\lambda > 310$ in terms of the calculated rates for the molecular elimination $H_2CO \rightarrow H_2 + CO$, the bond fission $H_2CO \rightarrow H + HCO$, and the intramolecular hydrogen abstraction $H_2CO \rightarrow H \ldots HCO \rightarrow H_2 + CO$ taking place in the electronic ground state. This work demonstrated consistency between experiment and theory. Consistency with the rates of formaldehyde pyrolysis and of the reaction H + HCO

= H_2 + CO was also obtained (Troe, 2007b; Troe and Ushakov, 2007). The quantum yields were represented in analytical form such that values outside the available experimental range can be predicted.

References

Calvert, J. G., Atkinson, R., Kerr, J. A., Madronich, S., Moortgat, G. K., Wallington T. J. and Yarwood, G.: *The mechanisms of atmospheric oxidation of the alkenes*, Oxford University Press, New York, 2000.

Calvert, J. G., Derwent, R.G., Orlando, J. J., Tyndall, G. S., and Wallington, T. J.: *The mechanisms of atmospheric oxidation of the alkanes*; Oxford University Press, New York, 2008.

Calvert, J. G., Mellouki, A., Orlando, J. J., Pilling, M.J. and Wallington, T. J., *The mechanisms of atmospheric oxidation of the Oxygenates*; Oxford University Press, New York, 2011.

Cantrell, C. A., Davidson, J. A., McDaniel, A. H., Shetter, R. E., and Calvert, J. G.: J. Phys. Chem. 94, 3902, 1990.

Clark, J. H., Moore, C. B., and Nogar, N. S.: J. Chem. Phys., 68, 1264, 1978.

Crow, M. B., Gilchrist, A., Hancock, G., Peverall, R., Richmond, G., Ritchie, G. A. D., and Taylor, S. R.: J. Phys. Chem. A, 113, 6689, 2009.

DeMore, W. B.; Sander, S. P.; Howard, C. J.; Ravishankara, A. R.; Golden, D. M.; Kolb, C. E.; Hampson, R. F.; Kurylo, M. J.; Molina, M. J. NASA Panel for Data Evaluation, Chemical Kinetics and Photo- chemical Data for Use in Stratospheric Modeling, JPL Publication 97-4, 1997.

Green, W. H., Moore, C. B., and Polik, W. F.: Ann. Rev. Phys. Chem., 43, 591, 1992.

Gratien, A.; Nilsson, E.; Doussin, J. F.; Johnson, M. S.; Nielsen, C. J.; Stenstrøm, Y.; Picquet-Varrault, B. J. Phys. Chem. A, 111, 11506, 2007.

Gorrotxategi Carbajo, P.; Smith, S. C.; Holloway, A. L.; Smith, C. A.; Pope, F. D.; Shallcross, D. E.; Orr-Ewing, A. J. J. Phys. Chem. A, 112, 12437, 2008.

Gratien, A., Pichet-Varrault, B., Orphal,.J., Perraudin and Doussin, J-F., J. Geophys. Res.112, D053005, (2007).

Horowitz, A. and Calvert, J. C.: Int. J. Chem. Kinet., 10, 805, 1978.

Lewis, R. S., Tang, K.Y., and Lee, Y. K. C.: J. Chem. Phys., 65, 2910, 1976.

Marling, L.: J. Chem. Phys., 66, 4200, 1977.

Meller, R. E. and Moortgat, G. K.: J. Geophys.Res., 105, 7089, 2000.

Motsch, M., Schenk, M., Zeppenfeld, M., Michael, S., Meerts, W. L., Pinkse, P. W. H., and Rempe, G.: J. Mol. Spectrosc., 252, 25, 200

Moortgat, G K. and Schneider, W., unpublished data cited in IUPAC Supplement III 1988.

Moortgat, G. K. and Warneck, P.: J. Chem. Phys., 70, 3639, 1979.

Moortgat, G. K., Seiler, W., and Warneck, P., J. Chem. Phys. 78, 1185, 1983.

Pope, F. D.; Smith, C. A.; Ashfold, M. N. R.; Orr-Ewing, A. J.
Phys. Chem. Chem. Phys., 7, 79−84, 2005a.

Pope, F. D.; Smith, C. A.; Davis, P. R.; Shallcross, D. E.; Ashfold, M. N. R.; Orr-Ewing, A. J. Faraday Discuss., 130, 59−72, 2005b.

Sander, S. P., Abbatt, J., Barker, J. R., Burkholder, J. B., Friedl, R. R., Golden, D. M., Huie, R. E., Kolb, C. E., Kurylo, M. J., Moortgat, G. K., Orkin V. L., and Wine, P. H.: Chemical Kinetics and Photochemical Data for Use in Atmospheric Studies, Evaluation No. 17; Jet Propulsion Laboratory: Pasadena, CA, USA, 2011.

Smith, G. D., Molina, L. T., and Molina, M.: J. Phys.Chem A, 106, 1233, 2002.

Smith, C.A., Pope, F. D., and Orr-Ewing, A. J.: J. Phys.Chem. A, 110, 11645, 2006.

Tang, K. Y., Fairchild, P. W., and Lee, E. K. C.: J. Phys. Chem. 83, 569, 1979.

W. H. Green, Moore C. B., and Polik, W. F.: Ann. Rev. Phys. Chem., 43, 591, 1992.
Tatum Ernest, C.; Bauer, D.; Hynes, A. J., J. Phys. Chem. A,116, 5910, 2012a.
Tatum Ernest, C.; Bauer, D.; Hynes, A. J., J. Phys. Chem. A, 116, 6983, 2012b.
Troe, J., J. Phys. Chem. A, 111, 3868 (2007a),
Troe, J., J. Phys. Chem. A, 111, 3862 (2007b)
Troe, J. and Ushakov, V. G., J. Phys. Chem. A, 111, 6610 (2007)

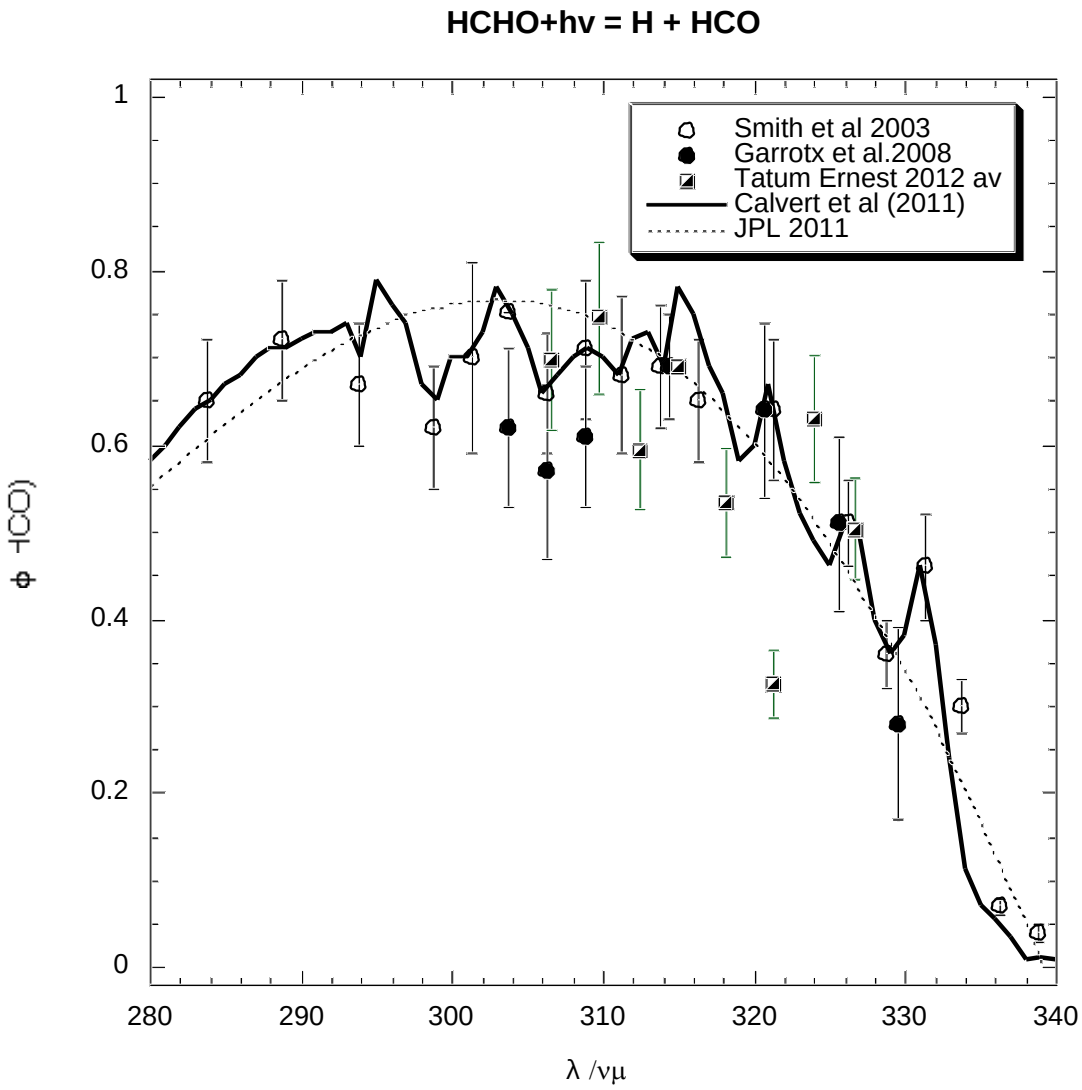

Figure 1: Experimental quantum yields for the 'radical' channel ϕ_1, from high resolution studies

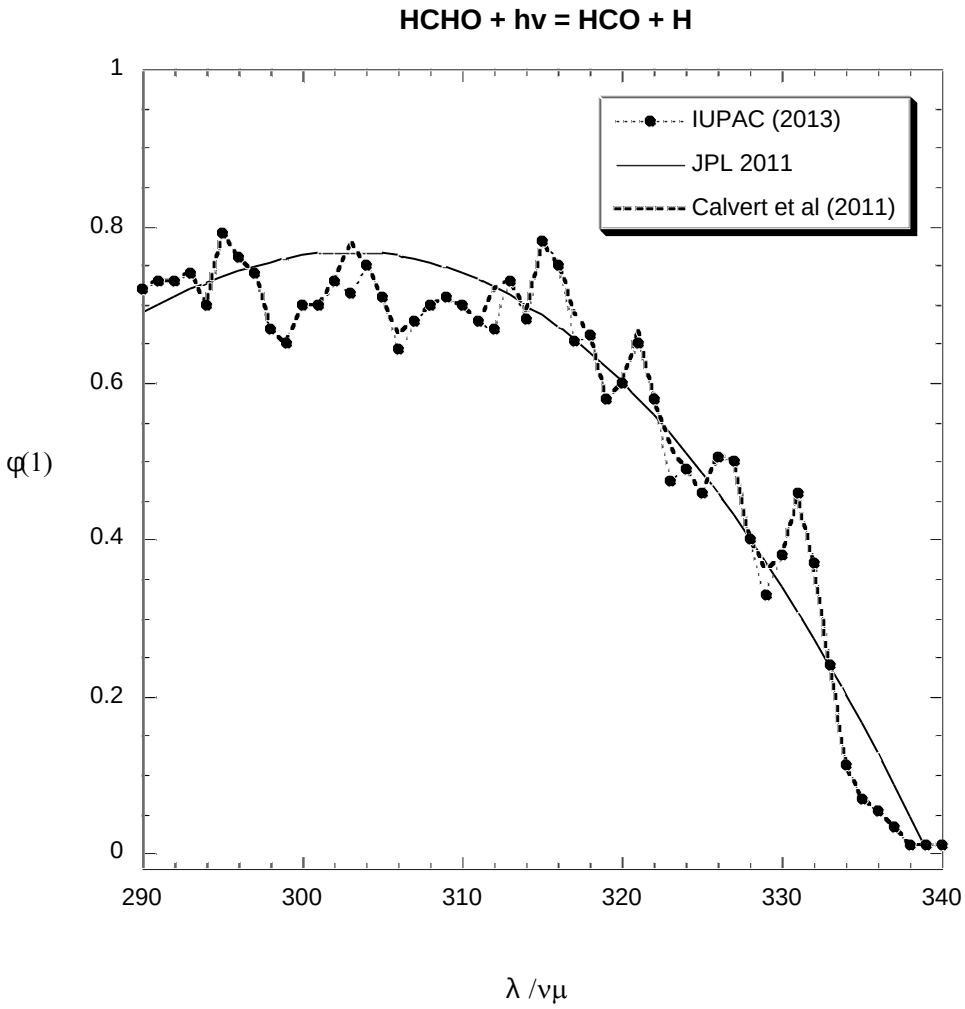

Figure 2: Comparison of quantum yields for the 'radical' channel $\phi_{1,}$ from recent evaluations

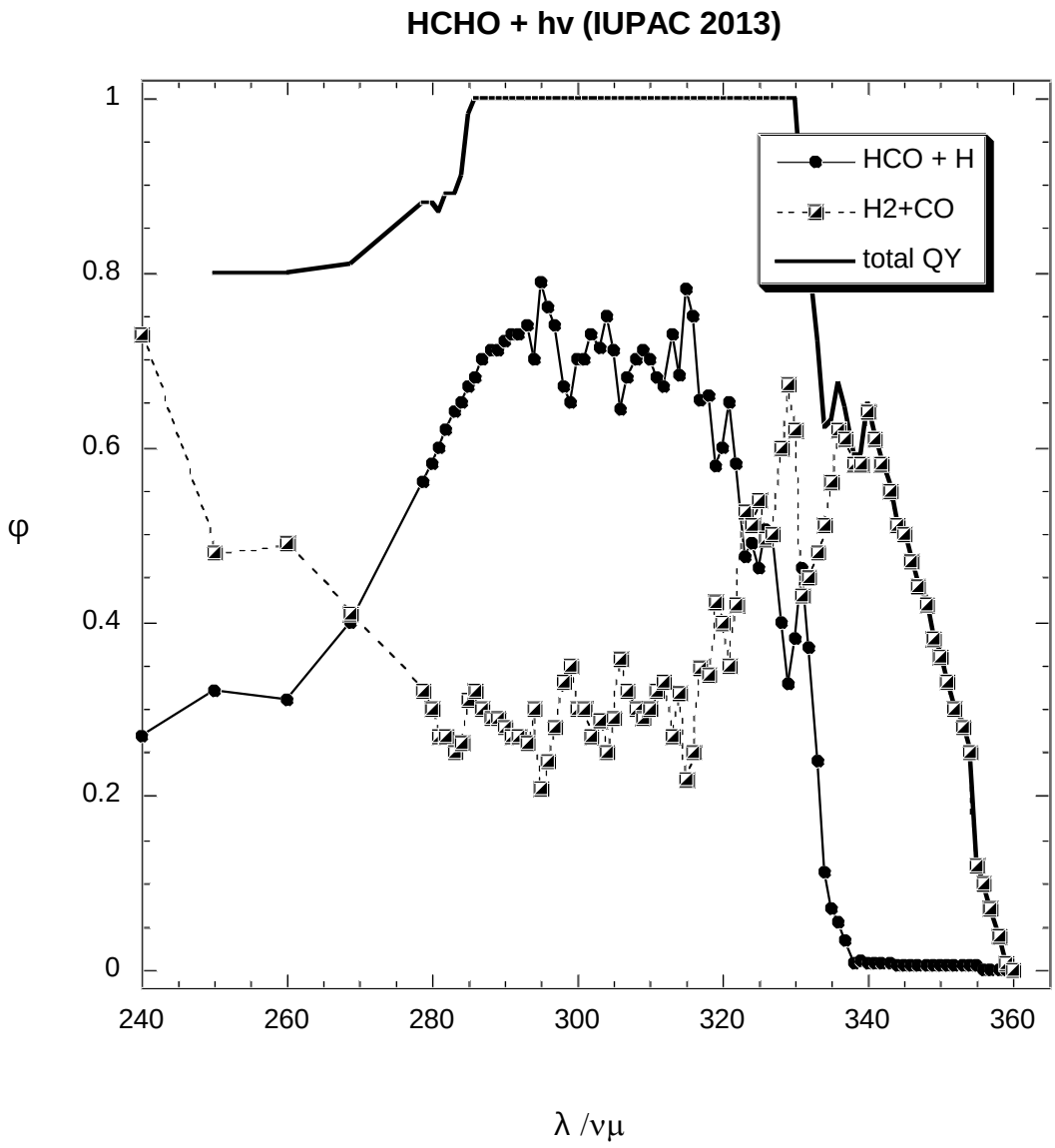

Figure 3: IUPAC recommendation for channel specific quantum yields